Cost-Effective Pipeline for a Rational Design and Selection of Capsaicin Analogues Targeting TRPV1 Channels

Daniel Bustos, Christian Galarza, Wilson Ordoñez, Sebastian Brauchi, and Bruna Benso*

Cite This: ACS Omega 2023, 8, 11736–11749

Read Online

ACCESS | Metrics & More | Article Recommendations | SI Supporting Information

ABSTRACT: Transient receptor potential (TRP) channels constitute a large group of membrane receptors associated with sensory pathways in vertebrates. One of the most studied is TRPV1, a polymodal receptor tuned for detecting heat and pungent compounds. Specific inhibition of the nociceptive transduction at the peripheral nerve represents a convenient approach to pain relief. While acting as a chemoreceptor, TRPV1 shows high sensitivity and selectivity for capsaicin. In contrast to the drugs available on the market that target the inflammatory system, TRPV1 antagonists act as negative modulators of nociceptive transduction. Therefore, the development of compounds modulating TRPV1 activity has expanded dramatically over time. Experimental data suggest that most agonist and antagonist drugs interact at or near capsaicin's binding site. In particular, the properties of capsaicin's head play an essential role in modulating potency and affinity. Here, we explored a cost-efficient pipeline to predict the effects of introducing chemical modifications into capsaicin's head region. An extensive set of molecules was selected by first considering the geometrical properties of capsaicin's binding site and then molecular docking. Finally, the novel ligands were ranked by combining molecular and pharmacokinetic predictions.
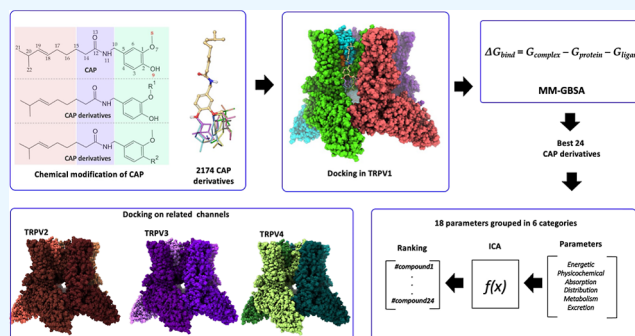
1. INTRODUCTION

Transient receptor potential (TRP) ion channels are a group of membrane proteins that respond to a wide range of sensory stimuli, constituting integral components of sensory transduction and cell signaling.[1−3] The original TRP gene was initially described in *Drosophila melanogaster* in 1989[4] and eventually led to the discovery of a large family of ion channels in vertebrates.[5] After 30 years of intense research, a unifying mechanism for TRP channel activation remains elusive.[6−9] The molecular detectors encoded in TRP channels are seemingly interlinked, conferring polymodal properties and promoting activation by various types of passing stimuli such as heat, changes in pH or voltage, and binding of a variety of ligands.[10] Here, we focus on TRPV1, the most studied thermal detector in the nociceptive system.[11−14] The capsaicin-sensitive TRPV1 channel is well expressed in sensory nerves, acting as a molecular detector for potentially harmful signals in primary sensory fibers.[15,16]

Along with their role as molecular sensors in the nociceptive pathway, evidence indicates that TRPV1 channels have a broad physiological function, underscoring their importance in pharmacology and biomedicine.[17,18] In contrast to commercially available drugs targeting the inflammatory system, TRPV1 antagonists act as critical negative modulators of nociceptive transduction.[19] Moreover, TRPV1 activation is followed by nerve inactivation,[2,13,14] making both potent

agonists and antagonists viable tools to promote the desired analgesic effect, provided the necessary pharmacokinetic characteristics are favorable.[19,20] In this context, the naturally occurring molecules capsaicin (CAP) and resiniferatoxin (RTx) are well-described vanilloid ligands acting as potent TRPV1 agonists.[9,21−23] On the other hand, capsazepine (CPZ), a synthetic derivative of CAP, is an inhibitor of TRPV1 activity.[24,25] All three have inhibited nociceptive neuron firing *in vitro* and *in vivo*.[26−28] Thus, targeting TRPV1 channel activity presents an attractive approach to pain relief that may qualify as the next generation of analgesics.[2,19,20]

Structural data unveiled the different coordinations used by these ligands, highlighting differences beyond interacting amino acids, including the geometrical constraints and electrostatic properties.[23,26] Notably, the interactions established by the polar head groups exhibited by TRPV1 ligands recruit amino acids in regions participating in the gating and
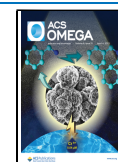
Table 1. Available TRPV1 Structures

| PDB ID	resolution (Å)	method	ligand	year	organism	expression System	mutation
7RL0	3.81	Cryo-EM	Capsaicin	2021	*Ictidomys tridecemlineatus* (squirrel)	*Homo sapiens*	no
7LPD	3.55	Cryo-EM	Capsaicin	2021	*Rattus norvegicus*	*Homo sapiens*	no
5IRX	2.95	Cryo-EM	DkTx & RTX	2016	*Rattus norvegicus*	*Homo sapiens*	no
					Haplopelma schmidti	*Escherichia coli* BL21(DE3)	
5IRZ	3.28	Cryo-EM	6OE, 6O8, 6ES	2016	*Rattus norvegicus*	*Homo sapiens*	no
5IS0	3.43	Cryo-EM	capsazepine	2016	*Rattus norvegicus*	*Homo sapiens*	no
3J5P	3.27	Cryo-EM	APO	2013	*Rattus norvegicus*	*Homo sapiens*	no
3J9J	3.27	Cryo-EM	APO	2015	*Rattus norvegicus*	*Homo sapiens*	no
3J5Q	3.80	Cryo-EM	DkTx & RTX	2013	*Rattus norvegicus*	*Homo sapiens*	no
					Chilobrachys guangxiensis		
3J5R	4.20	Cryo-EM	Capsaicin[a]	2013	*Rattus norvegicus*	*Homo sapiens*	no

[a]CAP molecule poorly solved.
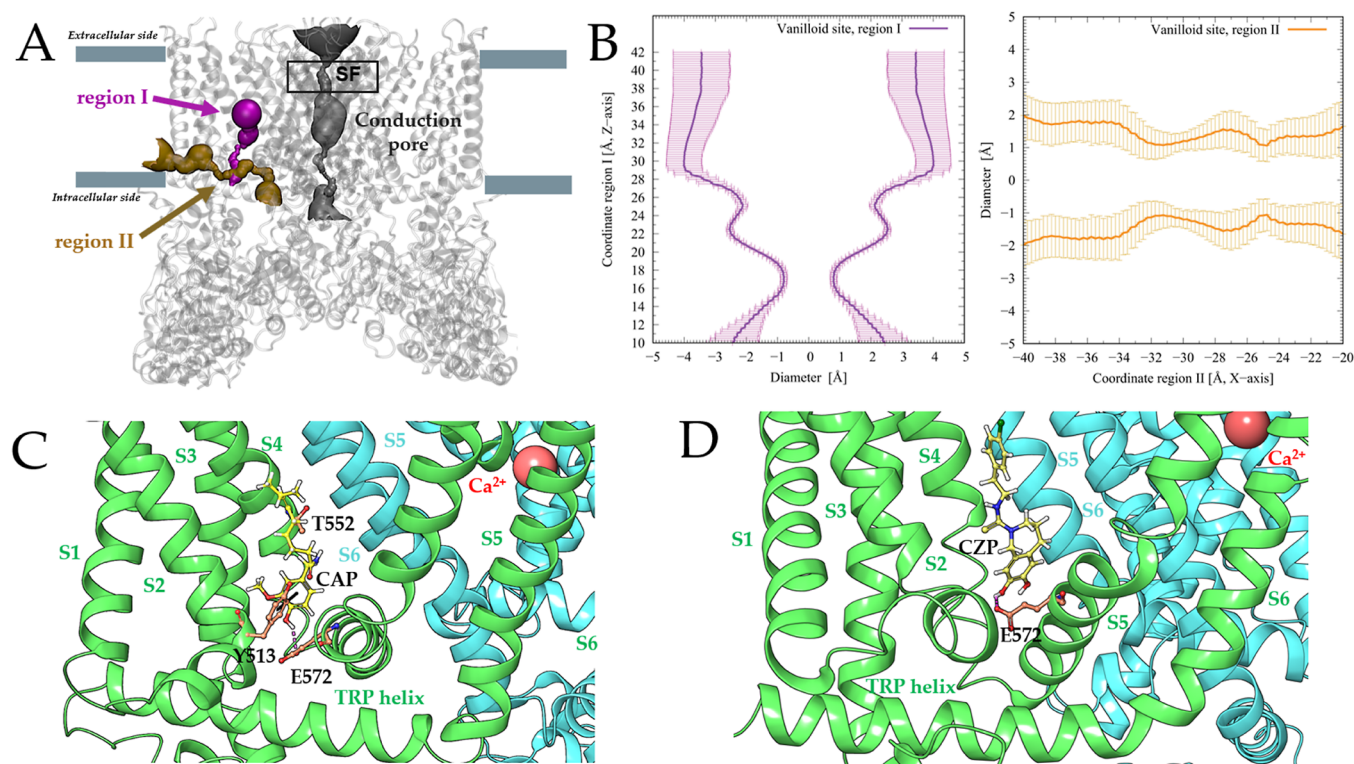
Figure 1. Vanilloid-binding site dimensions. (A) shows three different sites in the TRPV1 channel; the conduction pore is presented along the transmembrane helix with a volumetric representation in gray color and the vanilloid-binding site formed by two adjoining regions in purple and orange color. (B) represents the average ±standard deviation of the vanilloid-binding site dimensions located in regions I and II in parallel and orthogonal positions regarding the conduction pore, respectively. (C,D) are depicted as the binding site of capsaicin (CAP) and capsazepine (CZP) molecules into the TRPV1 structure (PDBs id: 7LR0 and 5IS0). Both molecules are stabilized by HB interactions (dashed pink line) with the residue E572.

modulation of the channel.[21,22,29] In this context, small molecules from the secondary metabolism of land plants containing groups similar to those on the CAP's head appear to provide a modular scaffold helpful for the straightforward design of potent and selective ligands for TRPV1.[27,28] Ideal for drug design, CAP's head derivatives are well recognized for the easiness of incorporation into pharmacophores, facilitating repurposing while keeping significant water solubility.[30,31]

Here, we aimed to find an economic computational pipeline to combine physicochemical data from *in silico* analysis with useful pharmacological descriptors. To this end, we devised a multiparameter algorithm considering affinity, pharmacokinetics properties, and target selectivity. As a proof of concept, we studied a large set of capsaicin-derived molecules by first

considering the geometric complementarity with TRPV1's binding pocket, explored the effects of introducing modifications into capsaicin's head region, and provided extensive energetic, physicochemical, and pharmacological predictions.

2. RESULTS

2.1. Geometrical Analysis of TRPV1's Vanilloid-Binding Site and the Design of Capsaicin Analogues. *2.1.1. Description of Capsaicin Hosting Volume.* The complete three-dimensional topology and subunit organization of TRPV1 in the apo (PDB ID: 7LQY[29]) and capsaicin-bound conformations (PDB ID: 7LR0[51] and 7LPD[52]) have been recently released. This data agrees with previously released cryoelectron microscopy (cryo-EM) datasets that also

addressed conformational differences between apo and ligand-bound states for CPZ, RTX, or the double-knot toxin DkTx (Table 1). In the absence of capsaicin, TRPV1 displays electron densities compatible with lipid molecules occupying the vanilloid-binding site, suggesting a competition between capsaicin and native lipids.[53,54] We did not include specific lipids explicitly bound to the structure in our simulations.

50 ns of fully atomistic molecular dynamics (MD) simulations were performed in the TRPV1 channel (PDB id: 7RL0), including membrane lipids, water molecules, and ions. The properties of the head play an essential role in modulating potency and affinity by coordinating residues located at the lower end of transmembrane helices S3 and S4.[22] Thus, the ligand-hosting cavity defines a volume that provides side chains coordinating CAP's head groups and stabilizing aliphatic chains[23,54,55] that can be further divided into regions named: regions I and II (Figure 1A). Region (I) is a volume that runs parallel to the conduction pore with the S3, S4, S5, and S6 helix boundaries. It extends for about 32 Å from the TRP helix upward, with a maximum diameter (~8 Å) at the level of the pore's central cavity below the selectivity filter (SF) (Figure 1A,B). The second region (II) is defined by the S1, S2, and the TRP helix running perpendicular to the conduction pore. The narrowest constriction of the cavity (~1.6 Å) coincides with the narrowest constriction of the pore at the level of the lower gate with an average diameter of 1.5 Å, the outer end of region II connects with the lipid membrane (Figure 1A,B). The vanillyl moiety of the CAP head accommodates polar residues of the loop S2−S3 and the S4−S5 linker surrounding the TRP helix,[35] where E572 (E570 in hTRPV1) interacts with CAP (Figure 1C).

The vanillyl moiety of the CAP head accommodates polar residues of the loop S2−S3 Y513 (Y511 in hTRPV1) through π−π interactions and with the S4−S5 linker surrounding the TRP helix,[35] where E572 (E570 in hTRPV1) interacts with CAP through a hydrogen bond (HB) (Figure 1C). Thus, it was demonstrated that hydrophobic residues such as F543 (tail), polar residues such as T550 (neck), and the negatively charged E570 (head) form HB with capsaicin to stabilize the binding and the open state of TRPV1.[22,55] On the other hand, the synthetic competitive antagonist CPZ occupies the same vanilloid-binding site of CAP, maintaining a key interaction with E572 through its polar head (Figure 1D).[21] Capsaicin differed from capsazepine substantially in the head group interacting with the Y513 residue through hydrogen bonding.

2.1.2. Computational Chemical Synthesis. Using the geometrical boundaries obtained, we found 2174 new molecules from modifying atoms eight or nine from the CAP's head. In both cases, we added polar chemical substitutes (Figure 2). We considered stereoisomers and the different protonation states at pH 7.4. Therefore, the initial pool was increased to 7369 molecules.

2.1.3. Docking Simulations and Highest-Scoring Molecules. The selected molecules were docked into the TRPV1 channel (PDB id: 7RL0). 66.919 docking poses were obtained from the ligands (Figure 3A). The docking simulations suggest a common binding mode that agrees with CAP's "tail up, head down" configuration into the binding site (Figure 3A,B).

The compounds were first docked and scored, selecting the best 70 docking poses (one per analogue). Then, these poses were rescored by MM-GBSA calculations to obtain the binding free energy (ΔGbind). The ΔGbind of CAP was used to normalize the values obtained. This strategy rendered 24 CAP
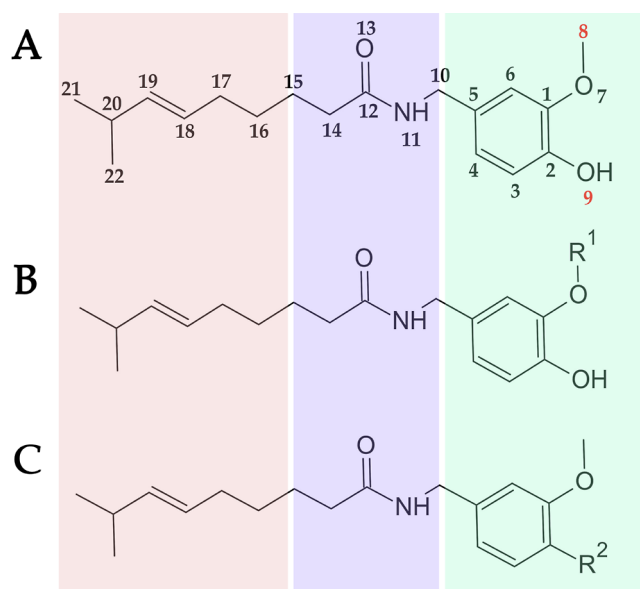

Figure 2. Capsaicin modifications. (A) Chemical modifications introduced into the head region of the CAP structure (embedded into the green rectangle) in atoms 8 and 9 to (B) R1 and (C) R2 substituents, respectively. The tail and neck regions (highlighted by the pink and purple rectangles) were not modified.

derivatives. Twenty have a substituent radical, replacing the methyl group (atom 8) of CAP, and four with a substituent in the hydroxyl group (atom 9) (Table 2).

The whole set of 24 molecules was found in the vanilloid-binding site, close to residues in the TRP domain helix, a region inaccessible by CAP and CZP due to its shorter length than our compounds. The CAP's interaction patterns found in the cryo-EM structure (PDB id: 7LR0) and corroborated by docking experiments are also found in our CAP analogues, where the head is stabilized by Y513 and E572 similar to CAP and CZP (Figure 3B,C).

2.2. Chemical Evaluation and Pharmacokinetics Predictions of Candidate Compounds. *2.2.1. Physicochemical Characteristics of Compounds.* Specific physicochemical characteristics must be considered and evaluated for a drug to be successful during its development.[53] Table 3 shows Lipinski's rule of five (ROF) and Veber's properties commonly employed to assess the pharmacokinetic characteristics in the drug design field.[56] We used the cutoff values defined by Lipinski as follows: molecular weight (MW) ≤ 500; octanol/water partition coefficient [log P(n-octanol/water) ≤ 5; the number of hydrogen bond donors (HBDs) ≤ 5; the number of hydrogen bond acceptors (HBA) ≤ 10, and those as per Veber's rule: rotatable bonds (RotB) ≤ 10, polar surface area (PSA) ≤ 140 Å² (or HBD + HBA ≤12)]. A good score on this set of physicochemical properties will favor the chances of a proposed drug being orally bioavailable.

All of our CAP analogues show 0 violations in Lipinski's ROF, similar to CAP and CZP, and even better than the RTX compound, which, due to its large size, has a higher MW (>500) and an octanol partition coefficient higher than 5. One key descriptor to calculate the LogP coefficient is a solvent-accessible surface area.[56] Due to the larger size of our compounds compared to CAP, it is expected that they will have a higher value of SASA. Nonetheless, the compound with the highest SASA value (2B) is only 23.51% higher than the SASA value of CAP. Due to the proposed chemical
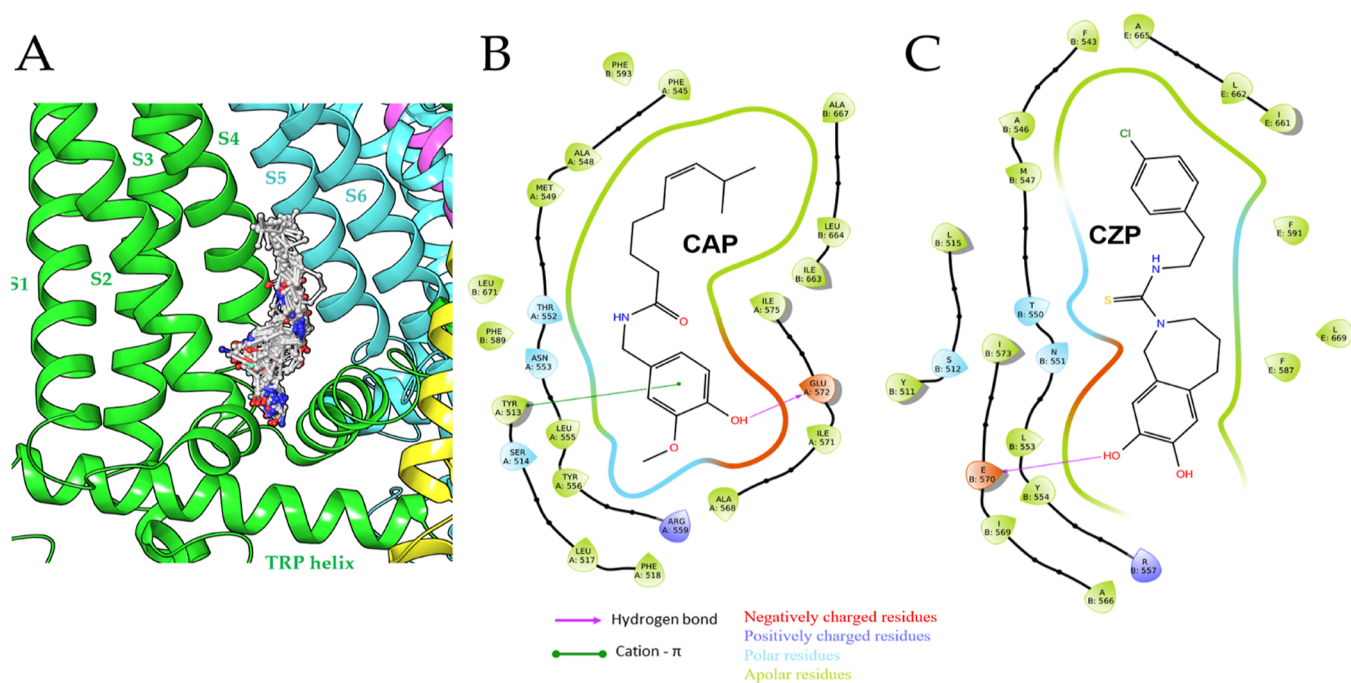
Figure 3. Capsaicin derivatives in their binding site. In (A), the best 24 compounds selected through the pipeline are positioned into the vanilloid-binding site in a "tail up, head down" configuration. 2D representation of the binding site of (B) CAP and (C) CZP molecules docked into the TRPV1 channel. The numbering of the structure of TRPV1 in the presence of CAP begins two positions after that in TRPV1 in the presence of CZP because they belong to different organisms described in Table 1.

modifications, we obtained 17 more hydrophilic compounds than CAP and seven more lipophilic compounds. However, according to Lipinski's ROF, our compounds have a LogP below 5. Likewise, the propensity to form hydrogen bonds is equal to or higher than CAP. Another widely employed rule is Veber's;[56] in this case, our CAP analogues have more rotatable bonds than Veber's rule suggested, resulting in a violation. It has been reported that an increased number of HBA and HBD associates with a poorer permeation. Likewise, higher PSA values are related to bad adsorption in drugs;[57] none of these parameters is the case with our compounds. Consequently, our compounds exhibit suitable pharmacokinetic parameters, measured as a function of ROF and Veber's descriptors.
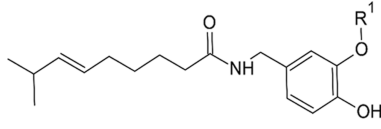
2.2.2. Prediction of ADME Qualities. The pharmacokinetic properties of drugs are considered one of the best criteria to predict their efficacy within the human body. For this, the adsorption, distribution, metabolism, and excretion (ADME) qualities of every CAP analogue were predicted with Qikprop and the pkCSM online server.[33] Table 4 provides the scores obtained for the 24 compounds used. To evaluate the bioavailability of drug-like molecules based on their pharmacokinetic properties, Jorgensen's rule of three (ROT) is widely used in the field.[41,57] The ROT states that LogS > −5.7 (S in mol/dm³), Caco-2 > 22 nm/s, and #Metab >7. 22 of 24 compounds were compliant with Jorgensen's ROT, ensuring good oral bioavailability (0 or 1 ROT violation).
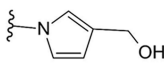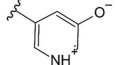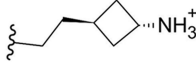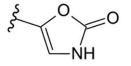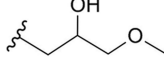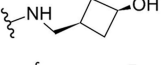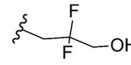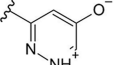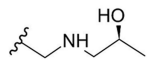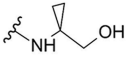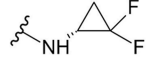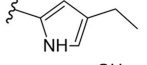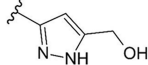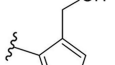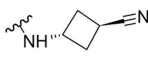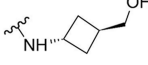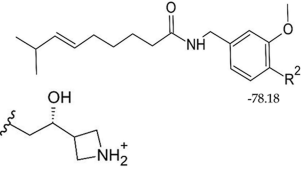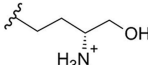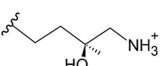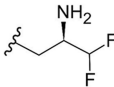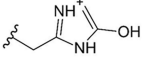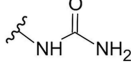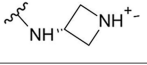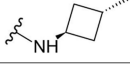
2.2.3. Absorption Properties. The solubility of a drug is a key property to assess the desired concentration of the drug in the human body. Consequently, the aqueous solubility must be evaluated early in drug design. Twenty compounds have LogS higher than −5.7, complying with the cutoff value proposed in the ROT. Skin is the body's largest organ, crucial to the permeation of topic drugs. The transdermal drug delivery was measured as the percent of human oral absorption and skin permeability. Using RTX as a cutoff, we obtained 15 compounds with better % HOA than RTX, eight of which have 100% oral absorption. All our compounds are within the accepted range (−8 to −1) regarding skin permeability. Another relevant parameter to assess the adsorption ability of any drug is the Caco-2 cell permeability, which is used to mimic the intestinal epithelium in the human body. Here, our CAP analogues show a good cell permeability of Caco-2 cells with values over the minimum (22 nm/s); even the compound with the lowest Caco prediction (10A) has nearly double the minimum (40.32 nm/s).

2.2.4. Distribution Properties. Once the drug is absorbed through systemic circulation or direct administration, the next step is to evaluate how the drug will be distributed into the interstitial and intracellular fluids. The brain−blood barrier (BBB) prevents the entry and accumulation of drugs into the brain. Consequently, BBB is the main limitation of the design of new drugs for the central nervous system. Here, we evaluated different measures of the BBB distribution, such as brain/blood partition coefficient (LogBB), MDCK cell permeability mimicking the BBB, and the central nervous system activity. The LogBB parameter indicates that 22 of our compounds are more polar than CAP, and even 12 are more polar than the RTX modulator. Similarly, the MCDK parameter confirms that 22 of the 24 compounds have poor permeability through MCDK cells compared with the CAP molecule. The activity in the central nervous system shows that all the molecules tested here are predicted to have scant activity, even the CAP, CZP, and RTX controls. These results suggest that our compounds have low odds of accumulation into the brain, avoiding secondary effects resulting from accumulation.

2.2.5. Metabolism Properties. In general, the active compounds of drugs are nonionized and lipophilic. However,

Table 2. Chemical Substituents for the CAP Structure[a]

Compound	Substituent (R¹)	MM-GBSA energy (kcal/mol)	Ratio: Compound/CAP	Compound	Substituent (R¹)	MM-GBSA energy (kcal/mol)	Ratio: Compound/CAP
1A	(pyrrole-CH2OH structure)	-98.97	1.52	14A	(pyridinium-O⁻ structure)	-68.88	1.06
2A	(cyclobutyl-NH3⁺ structure)	-79.46	1.22	15A	(oxazolone structure)	-68.84	1.06
3A	(OH, O-methyl structure)	-79.16	1.22	16A	(NH cyclobutyl-OH structure)	-66.62	1.02
4A	(F, F, OH structure)	-77.94	1.20	17A	(pyridazine-O⁻ structure)	-65.42	1.01
5A	(HO, NH structure)	-77.56	1.19	18A	(NH cyclopropyl-OH structure)	-65.35	1.00
6A	(NH cyclopropyl F,F structure)	-76.91	1.18	19A	(pyrrole ethyl structure)	-64.85	1.00
7A	(pyrazole-CH2OH structure)	-75.66	1.16	20A	(furan-CH2OH structure)	-64.43	0.99
8A	(NH cyclobutyl-N structure)	-74.50	1.15	1B	(OH azetidine-NH2⁺ structure)	-78.18	1.20
9A	(NH cyclobutyl-OH structure)	-72.31	1.11	2B	(NH3⁺, HO structure)	-77.21	1.19
10A	(H3N⁺, OH structure)	-72.14	1.11	3B	(NH⁺, NH, OH imidazoline structure)	-76.41	1.17
11A	(NH2, F, F structure)	-71.00	1.09	4B	(NH azetidine-NH⁺⁻ structure)	-66.65	1.02
12A	(NH, O, NH2 urea structure)	-70.37	1.08				
13A	(NH cyclobutyl structure)	-69.36	1.07				

[a]The substituents to R1 are distributed from the compound a1 to a20 and R2 from the compound b1 to b4. The binding free energies obtained for each complex were obtained from MM-GBSA calculations. The MM-GBSA energy to the CAP-TRPV1 complex is −65.06 kcal/mol.

after the distribution of the drug into the bloodstream, the drug can metabolize into a series of chemical modifications produced by enzymes, making the drug polar or hydrophilic and hence less active or even rapidly excretable. According to Jorgensen's ROT, drugs with good oral bioavailability must have no more than seven primary metabolites. Here, we evaluated 21 possible metabolic reactions for every compound. Seven CAP analogues have less than seven primary metabolites, similar to CAP and CZP; the other six have exactly seven primary metabolites. In humans, hepatic cytochrome P450 is critical for drug metabolism. Specifically, cytochrome P450 3A4 (CYP3A4) is a multifunctional enzyme highly related to metabolizing clinical drugs. It has been widely characterized in the scientific literature as the most important enzyme of the P450 enzymatic complex. CAP, RTX, and 17 of our compounds are likely metabolized by CYP3A4.

2.2.6. Excretion Properties. As we mentioned, the remnant drugs metabolized by the hepatic and/or intestinal enzymes transform lipophilic compounds into hydrophilic ones to facilitate their excretion through the two main routes, renal or biliary. Organic cation transporters are electrogenic proteins that mediate the passing of organic cations in the renal excretion system. OCT2 is a passive diffusion transporter that plays a major role in cationic drugs' basolateral uptake. We evaluated if our proposed compounds could act as an OCT2 substrate, where only one compound could be excreted by OCT2 protein. Total clearance (TC) describes the rate of drug excretion to the drug concentration in plasma as a combination of renal, biliary, and hepatic clearance. Zhivkova and Doytchinova[58] describe a cutoff to discriminate high, moderate, and low clearance as $\log(\text{TC}) \leq 0.48$, $0.48 \leq \log(\text{TC}) \leq 2$, and $\log(\text{TC}) \geq 2$. We found 16 compounds with

Table 3. Chemical Properties of Candidate Compounds[a]

					biological properties				
	MW	HBA	HBD	Log(Po/w)	SASA	ROF violations	RotB	PSA	Veber violations
1A	386.49	5	3	3.024	780.286	0	11	93.579	1
2A	388.55	5	4	3.500	806.451	0	12	94.336	1
3A	379.50	7	3	3.050	773.435	0	13	93.920	1
1B	388.55	4	3	4.551	789.203	0	12	73.995	1
4A	385.45	5	3	3.492	747.217	0	12	85.239	1
5A	378.51	7	4	2.084	746.571	0	13	95.492	1
2B	390.57	5	4	3.760	816.992	0	13	88.714	1
6A	382.45	4	3	4.212	745.366	0	11	81.718	1
3B	385.51	4	3	4.238	808.276	0	11	92.546	1
7A	387.48	6	4	2.630	776.996	0	11	114.21	1
8A	385.51	6	3	3.264	767.021	0	11	104.86	1
9A	390.52	6	4	3.278	778.820	0	12	100.91	1
10A	378.51	6	5	1.911	752.055	0	13	113.03	1
11A	384.47	5	4	3.206	754.797	0	12	89.197	1
12A	349.43	5	5	1.123	702.686	0	10	130.52	1
13A	374.52	4	3	4.078	726.458	0	11	79.287	1
14A	384.47	6	3	3.128	755.805	0	10	98.474	1
15A	374.44	6	3	2.047	704.580	0	10	121.79	1
4B	373.54	4	2	4.890	736.822	0	11	61.750	1
16A	390.52	6	4	3.152	753.415	0	12	98.248	1
17A	385.46	7	3	2.503	739.092	0	10	109.61	1
18A	376.50	6	4	3.095	780.565	0	12	95.113	1
19A	384.52	3	3	4.779	772.364	0	11	79.573	1
20A	387.48	5	3	3.374	735.191	0	11	93.698	1
CAP	305.42	4	2	3.522	661.441	0	9	68.417	0
CZP	376.90	4	3	3.796	618.235	0	3	65.738	0
RTX	638.72	10	2	6.009	915.474	2	8	125.941	0

[a]The compounds were ordered by the MM-GBSA energy (kcal/mol). MW: molecular weight (g/mol). HBA: no. of HB acceptor. HBD: no. of HBDs. Log(Po/w): octanol/water partition coefficient. SASA: Solvent-accessible surface area ($Å^2$). No. of violations under Lipinski's ROF. RotB: no. of rotatable bonds. PSA: polar surface area ($Å^2$) and no. of violations under Veber's rule.

moderate clearance similar to CAP and 8 with a lower clearance index.

2.3. Multiparameter Method to Rescore the Candidates. Aiming to obtain a prediction based on our different calculations, we prepared a simple algorithm allowing us to rescore all 24 ligands according to the different physicochemical and pharmacokinetic values presented. Tables S1 and S2 show the results obtained, respectively. In particular, Table S1 presents the weights with which each group contributes a score measure of interest. Of the latter, we can see that binding energy has an importance of only 10% for constructing our score measure. At the same time, the physicochemical, absorption, and distribution characteristics are the most important (around three times).

On the other hand, the characteristics of the metabolism and excretion groups are the least important, with a weight of 3 and 1%, respectively. On the other hand, Table S2 shows the results of the correlations of the auxiliary variables for the characteristics with the score measure, with the first column being the contribution to the general score and the second its contribution to its group. From this table, we can see that the results for binding energy are consistent with the literature since it has a negative value (i.e., favorable); the lower its quantity, the better the compound. On the other hand, we have the variable HBA, which has a positive effect concerning the score measure of 0.06 when HBA <5 and 0.04 for values greater than 5. Note that, for variable CYP3A4, the correlation looks weakly positive, so there was a slight trend of higher

scores when it took the value of "yes". It is worth emphasizing that this multiparametric scoring method (MSM) considers the relationships between the characteristics, so the rules usually considered individually by characteristic are not necessarily satisfied. Lastly, Table 5 presents the 24 compounds ordered from best to worst according to the score measure determined by our MSM. Our data and MSM analysis suggest that the best four compounds were 10A, 12A, 5A, and 1A.

2.3.1. MD Simulations of the Best-Scored Compounds. We evaluated the coordination of our four best-scored compounds (10A, 12A, 5A, and 1A) with TRPV1 through 100 ns of MDs and compared them against the CAP-bound and CZP-bound TRPV1 complexes. First, our simulations showed a correct correlation with the intermolecular interactions found in the cryo-EM structures for CAP and CZP (PDB ids: 7LR0 and 5IS0). Specifically, the CAP's neck interacts with T552 and N553 through HBs, whose interaction fraction (number of interactions per frame divided into the whole simulation time) for T552 and N553 is 72.26 14.43%, respectively (Figure 4A). Similarly, the CAP's head interacts with the E572 *via* HBs or HBs mediated by water molecules. In contrast, the CZP molecule maintains significantly fewer interactions during the simulation time than CAP. HBs stabilize CZP's head with E572, S514, and V585 (Figure 4B). R559 interacts simultaneously with CZP's head and neck; this is not observed in the simulations of CAP. The four CAP analogues maintain the classical interactions with Y513, T552,

Table 4. Evaluation of ADME Properties for the Drug Proposed Compounds[a]

	absorption				distribution			metabolism		excretion		
	LogS	% HOA	LogKp	Caco	LogBB	MDCK	CNS	#Metab	CYP3A4	TC	OCT2	ROT
1A	−3.88	76.43	−4.38	59.61	−1.55	41.54	−2	6	yes	1.398	no	0
2A	−4.12	79.98	−4.50	65.80	−1.54	49.39	−2	7	yes	1.405	no	1
3A	−4.61	93.73	−1.98	541.67	−1.73	324.74	−2	8	no	1.484	no	1
1B	−5.93	100.00	−1.47	1250.32	−1.17	806.05	−2	7	yes	1.272	no	2
4A	−4.95	92.74	−2.39	341.71	−1.68	511.49	−2	7	yes	0.942	no	1
5A	−2.41	70.53	−4.64	56.71	−1.57	40.76	−2	8	yes	1.330	no	1
2B	−4.00	83.98	−4.09	90.45	−1.39	75.81	−2	9	yes	1.184	no	1
6A	−5.34	100.00	−1.92	630.21	−1.14	1272.40	−2	5	yes	1.182	no	0
3B	−6.40	100.00	−2.29	399.39	−1.77	247.71	−2	7	no	0.939	no	2
7A	−4.71	76.87	−3.40	84.89	−2.52	55.37	−2	6	yes	1.255	no	0
8A	−5.78	86.38	−2.88	179.10	−2.03	123.37	−2	6	yes	1.240	no	1
9A	−4.65	90.42	−2.40	298.00	−1.87	205.67	−2	6	no	1.299	no	0
10A	−2.54	66.87	−4.85	40.32	−1.91	24.12	−2	9	no	0.764	yes	1
11A	−3.87	80.42	−4.43	86.85	−1.16	143.19	−2	8	yes	1.158	no	1
12A	−3.23	62.77	−4.00	43.09	−2.44	36.48	−2	6	yes	1.182	no	0
13A	−4.94	100.00	−1.72	972.54	−1.12	659.84	−2	5	yes	0.987	no	0
14A	−4.80	83.59	−2.83	138.57	−2.12	95.29	−2	8	yes	0.952	no	1
15A	−3.90	71.97	−3.78	70.14	−2.29	45.00	−2	5	yes	1.214	no	0
4B	−5.63	100.00	−1.09	2396.09	−0.63	1764.60	0	6	no	1.240	no	0
16A	−3.89	88.09	−2.47	242.61	−1.80	201.27	−2	5	no	0.746	no	0
17A	−4.44	78.61	−3.14	116.77	−2.22	69.72	−2	7	yes	1.231	no	1
18A	−5.05	91.73	−2.35	404.93	−1.87	228.74	−2	6	no	0.943	no	0
19A	−6.06	100.00	−1.60	811.94	−1.29	537.22	−2	6	yes	0.989	no	1
20A	−4.81	95.61	−1.91	540.56	−1.57	304.82	−2	7	yes	1.294	no	1
CAP	−4.49	100.00	−1.66	1175.29	−0.90	837.03	−1	6	yes	1.398	no	0
CZP	−5.43	100.00	−2.53	705.21	−0.65	1418.00	−1	5	no	−0.44	no	0
RTX	−7.71	81.984	−2.36	360.82	−1.66	164.37	−2	11	yes	−0.03	no	2
min value	−6.5	0	−8.0	<25 (poor)	−3.0	<25 (poor)	−2 (inactive)	1	yes (bad)	NI	yes (bad)	
max value	0.5	100	−1.0	>500 (great)	1.2	>500 (great)	2 (active)	8	no (good)	NI	no (good)	

[a]The compounds were ordered by the MM-GBSA energy (kcal/mol). LogS: predicted aqueous solubility (mol/dm³). % HOA: percent of human oral absorption. LogKp: skin permeability (cm/h). Caco: apparent Caco-2 cell permeability (nm/s). MDCK: apparent MDCK cell permeability (nm/s). CNS: Central nervous system activity scale. #Metab: number of likely metabolic reactions. CYP3A4: isoform of cytochrome P450 metabolism. TC: total clearance of the drug [Log(mL/min kg)]. OCT2: organic cation transporter 2 as a renal uptake transporter.

N553, and E572 equally to CAP (Figure 4C−F). Surprisingly, our compounds also interact with R559, similar to CZP. Three of the four (10A, 5A, and 1A) compounds interact with Q702 located in the TRP helix mainly due to its length being more significant than the size of CAP. Another remarkable aspect is that the best compound (10A) has a charged amino group, which would help ionic interactions with E572 (Figure 4C).

2.3.2. Comparing the Selectivity of CAP Analogues in TRPV Channels. Aiming to explore whether our pipeline helps predict the selectivity of the tested compounds, we applied our channel to close relatives of TRPV1 (*i.e.*, TRPV2-4). To this end, we first evaluated the dimensions of the vanilloid-binding site in TRPV2-4 (Figure S1). The three-dimensional structure of the vanilloid-binding site of TRPV3 is significantly narrower than the rest of the channels evaluated, followed by TRPV4. Unlike the rest of the channels, TRPV2 shows a wide opening at the site without apparent constrictions.

As reported in the literature, TRPV2-4 channels are insensitive to the TRPV1 modulators: CAP and CZP.[18] Therefore we first tested whether TRPV1 ligands CAP, CZP, and RTX bind these receptors under our in silico conditions (Figure 5 and Table 6). Our docking assays agree with experimental observations that CZP cannot bind to the vanilloid-binding site in TRPV2-4. Similarly, CAP cannot bind to TRPV2 and 3. On the other hand, it has been

described that RTX is capable of transversely modulating TRPV1-4 channels; here, RTX was found on the site of all channels except TRPV3, a channel with a significantly narrower binding site than the rest (Figure S1).

In the spirit of completing the proposed pipeline, we took the best four scoring analogues obtained previously (10A, 12A, 5A, and 1A) and inspected whether they can bind to the vanilloid site of TRPV1-4 channels. We measured the average length in different conformers for all the ligands above, finding that the ligand with the maximum extension had 20 Å, ensuring that these molecules fit longitudinally (tail up, head down) within the vanilloid site in the four TRP channels analyzed. Unlike TRPV1, where all the compounds were well hosted by the vanilloid-binding site (Figure 5A), a marked selectivity for the compounds is not appreciated in the other TRPVs, except for compound 1A in the TRPV2 channel.

CAP analogues are distributed between the vanilloid-binding site in TRPVs (Figures 5 and S2) and a site that borders the lipid membrane at the exit of region II previously studied. This site has been described as another modulation site for TRPV's channels interacting with ligands such as the coumarin derivative osthole and 2-aminoethoxydiphenyl borate.[59,60]

Table 5. Multiparameter Method Scores Every CAP Analogue According to its Energetic, Physicochemical, and Pharmacokinetic Properties

compounds	score
10A	4.88
12A	4.71
5A	4.60
1A	4.39
7A	4.30
15A	4.18
2A	4.11
2B	3.84
17A	3.83
11A	3.56
14A	3.51
8A	3.48
9A	3.37
16A	3.34
3A	3.18
18A	3.08
4A	2.94
20A	2.75
3B	2.63
6A	2.26
13A	2.20
19A	2.02
1B	1.82
CAP	1.69
4B	1.34

3. DISCUSSION

Here, we explored a cost-efficient pipeline to score compounds as part of the drug design strategy. As proof of concept, we used TRPV1 receptors, for which we have different structural conformation states and also close relatives of TRPV1 (*i.e.*, TRPV2-4).[61] The extensive research performed on the capsaicin receptor allows us to evaluate well-described ligands as control conditions (*i.e.*, CAP, CZP, and RTX). We tested the effects of introducing a large set of chemical modifications into capsaicin's head region. The set of molecules was selected by first considering the geometrical properties of capsaicin's binding site in TRPV1, followed by molecular docking. Finally, by means of an open-source multivariable algorithm, we obtained four putative high-scoring analogues.

CAP is a natural derivative compound with a nonpolar phenolic structure, and capsaicinoids are acid amides of C9−C11 branched-chain fatty acids and vanillylamine.[62] Due to its chemical structure, capsaicin can be well absorbed when administered topically or orally, reaching 94% absorption.[63] The diversity of functional groups in the head, neck, and tail regions modulate CAP-derived ligands' potency, pharmacokinetics, and pharmacodynamic properties.[31] In particular, the properties of the head play an essential role in modulating potency and affinity by coordinating residues located at the lower end of transmembrane helices S3 and S4 and the linker S4−S5, reconfiguring the interaction between the linker and the TRP domain helix in a transition that is thought to be critical to promote the open conformation of the channel.[23] Experimental data suggest that most agonist and antagonist drugs interact at or near capsaicin's binding site. In particular, the properties of capsaicin's head play an essential role in modulating potency and affinity. Our MDs allow us to obtain geometrical constraints of the binding site. We found that our
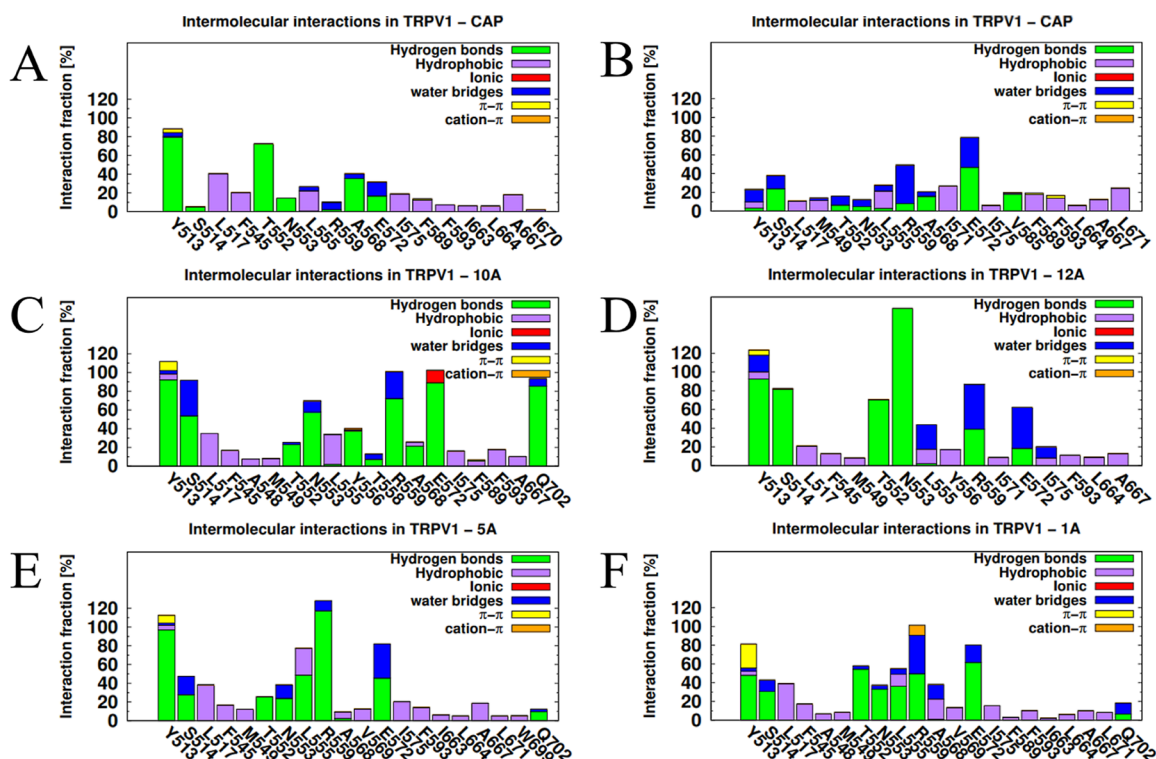

Figure 4. Intermolecular interactions between protein and ligand: (A−F) represent the intermolecular interactions of TRPV1 channel and capsaicin (CAP), capsazepine (CZP), and the CAP analogues 10A, 12A, 5A, and 1A calculated along with the simulation time (100 ns).
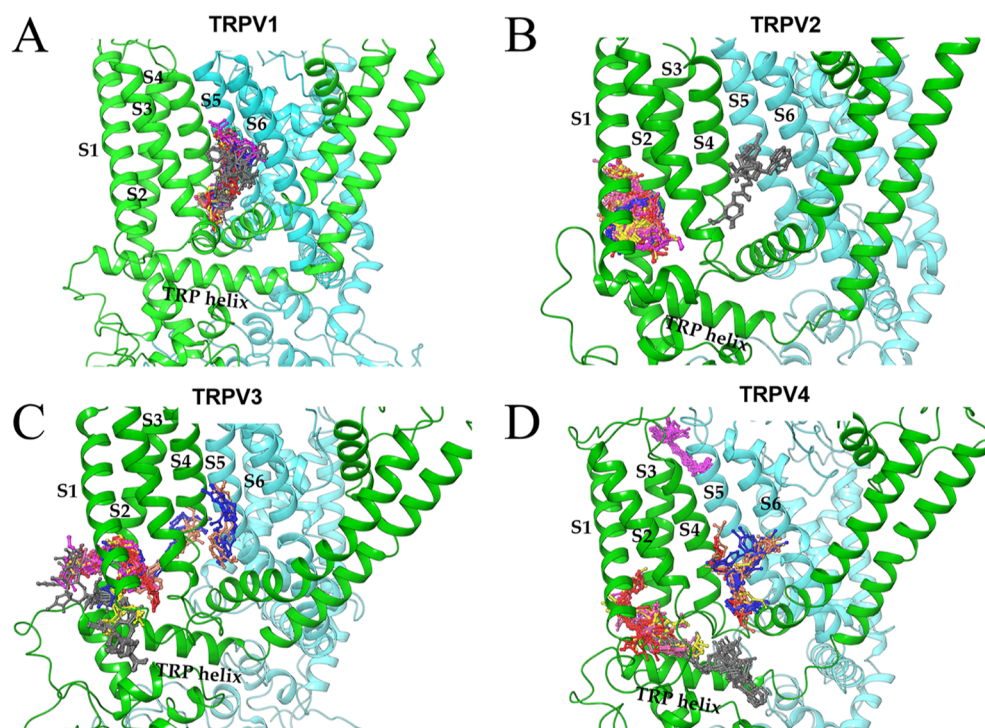
Figure 5. Clustering of all docking poses CAP (faded red−orange color), CZP (blue color), RTX (gray color), and the best four CAP analogues ranked by the MSM: 10A (magenta color), 12A (faded salmon color), 5A (red color), and 1A (yellow color) were docked into the monomer A of TRPV1 (PDB id: 7LR0), TRPV2 (PDB id: 6OO7), 5C is TRPV3 (PDB id: 6UW6), and 5D is TRPV4 (PDB id: 7AA5) channels. Green and cyan ribbons represent the monomers A and B of every channel, respectively. At most, 10 docking poses of each ligand are shown.

Table 6. Propensity to Find Ligands within the Vanilloid-Binding Site[a]

TRPV1	CAP	CZP	RTX	10A	12A	5A	1A
monomer A	100%	100%	100%	100%	100%	100%	100%
monomer B	100%	100%	100%	100%	100%	100%	100%
monomer C	100%	100%	100%	100%	100%	100%	100%
monomer D	100%	100%	100%	90%	100%	100%	43%
summary	true	true	true	true	true	true	true
TRPV2							
monomer A	0%	0%	100%	0%	0%	0%	100%
monomer B	0%	60%	100%	0%	0%	30%	100%
monomer C	0%	0%	30%	0%	0%	0%	30%
monomer D	0%	100%	100%	20%	0%	0%	100%
summary	false	false	true	false	false	false	true
TRPV3							
monomer A	20%	30%	0%	0%	0%	0%	0%
monomer B	0%	0%	70%	0%	0%	0%	0%
monomer C	20%	15%	100%	0%	0%	0%	30%
monomer D	30%	0%	43%	0%	0%	0%	10%
summary	false	false	false	false	false	false	false
TRPV4							
monomer A	100%	100%	0%	0%	0%	20%	10%
monomer B	100%	40%	88%	0%	17%	20%	50%
monomer C	100%	40%	100%	83%	89%	0%	80%
monomer D	100%	80%	86%	0%	0%	0%	0%
summary	true	false	true	false	false	false	false

[a]Percentages of the number of poses found within the vanilloid site over the total number of poses obtained for each monomer and ligand. The summary is marked as true when the ligand is found over 50% in at least three of the four monomers.

newly designed capsaicin analogues coordinate well with residues of the loop S2−S3 and S4−S5 linker surrounding the TRP helix. Specifically, E572 (E570 in hTRPV1), F543 (F541 in hTRPV1), and T550 (T498 in hTRPV1) are known

for establishing a direct interaction with CAP through hydrogen bonding and hydrophobic interactions.[55] In this context, E570—interacting with the ligand's head—would likely promote binding and stabilize the open state of TRPV1.

Studies on human TRPV1, where E570 has been replaced by polar residues (i.e., lysine or glutamine), retained capsaicin sensitivity.[16] Reinforcing the fundamental mechanisms to design novel ligands and the discovered hydrophobics' site involving F543 may serve us to predict analogue modulation activity. RTX is a significantly more extensive and complex molecule when compared to capsaicin. In agreement with its complexity, the binding site involves Y511, S512, L515, F543, M547, N551, and Y555.[64] All the mentioned residues interacted with the selected analogues 1A and 10A.

Most drugs exert their pharmacologic effects by binding receptors; however, to produce the desired pharmacologic effect, they should not only be structurally capable of interacting with the appropriate coordination but also reach the membrane receptor in the first place.[65] The pharmacokinetics of ADME has been extensively used to score new compounds in the pharmaceutical industry, and certain predictions can be drawn from this approximation.[66,67] Moreover, the physicochemical parameters must be considered and evaluated for ADME to reach a drug's successful development.[68] ADME properties guarantee end points that play an important role in distinguishing compounds that might represent a hazard or be impractical for their use in pharmacological treatments.[69] The multiparameter scoring method proposed here provides an excellent tool to assess and balance the distinct datasets in this article. It weighted the different physicochemical and pharmacokinetic values with an internal statistical reference. It proved efficient in providing a simple score calculation for any new set of compounds, simplifying the whole process of ligand selection. Moreover, the code containing the algorithm is suitable for custom modifications, simplifying the process of incorporating experimental results into the pipeline when available.

We found that the vanilloid-binding site has sufficient space to host our CAP derivatives; however, not all compounds meet ADME parameters. A final set of proposed ligands was obtained by weighting protein–ligand interactions from MDs and ADME properties. The compounds presented in the final shortlist not only present a favorable interaction with the receptor but also follow both the ROF and Veber's rules for physicochemical properties, ultimately ensuring that essential properties such as good oral bioavailability are conserved. Moreover, our bioinformatic study suggests that the best-scoring ligands will likely interact with TRPV1 with significant affinity and selectivity, distinguishing TRPV1 channels from the close relatives TRPV2-4. Considering the limitations of predictions in the absence of experimental data, our results must be taken cautiously. Further studies should provide experimental evidence for our bioinformatic predictions and the convenience of our multiparametric tool for drug design predictions on a larger scale.

4. MATERIALS AND METHODS

4.1. Simulation Details and Vanilloid-Binding Site Analysis.
We analyzed the dimensions of the vanilloid-binding site in the TRPV1 channel to propose chemical modifications to the CAP structure. The 3D coordinates of the TRPV1 channel were downloaded from the Protein Data Bank website with the PDB id: 7LR0.[32] The resolved ligands of CAP in each monomer and sodium ion into the SF were maintained in the structure. The channel was prepared in Maestro/Schrödinger suite, v.2021-1,[33] where the correct bond orders were assigned. The protonation states were adjusted with PropKa31 software

v.3.4.0[9] at pH 7.4. Energy minimization was performed to relax the structure using a convergence criterion of 0.3 Å between the heavy atoms of the protein. The OPM database[34] was used to orient the TRPV1 channel in the Z-axis, inserting a POPC (1-palmitoyl-2-oleoyl-sn-glycerol-3-phosphocholine) lipid bilayer surrounding the protein. The system was embedded into an orthorhombic box of single-point charge water molecules,[35] adding 150 mM NaCl to provide electroneutrality. Desmond presented the Maestro/Schrödinger suite, and the force field OPLS3e[36] was employed to perform 50 ns of MD simulation. Nosé–Hoover chain thermostat and Martyna–Tobias–Klein barostat methods were used to guarantee a temperature = 300 K and pressure = 1 atm, respectively, in an NPT ensemble. The standard nonbonded cutoffs in the Maestro/Schrödinger suite were employed. The HOLE v.2.2.005[37] analysis allows us to evaluate the dimension within the vanilloid-binding site formed by the S3, S4, S5, S6, and TRP helix in the TRPV1 channel. One hundred frames were collected (every 0.5 ns) from MDs. The vanilloid-binding site was divided into regions named: region I comprising the cavity occupied by the CAP molecule and formed by S3, S4, S5, and S6 helix, parallel to the conduction pore. Region II includes surfaces provided by the S1, S2, and TRP helix in an orthogonal position with respect to the conduction pore (Figure 1A,C). The dimensions of both regions were calculated independently, measuring every 0.25 Å in the Z-axis and X-axis for regions I and II, respectively.

4.2. Ligand Modification and Optimization.
The CAP molecule was obtained from the TRPV1 channel (PDB id: 7LR0) and used as a starting point to design chemical modifications. Aiming to evaluate modifications in CAP's head, modifications were introduced in the 4-hydroxy-3methoxyphenyl group at atoms 8 and 9. For each modification in R1 (atom 8) and R2 (atom 9): 2174 chemical fragments were attached independently, all filtered by the dimensions of the vanilloid-binding site. This chemical library is available in the custom R-group enumeration tool in the Maestro/Schrödinger suite. The new CAP derivatives were prepared in the Ligprep tool at pH 7.4 under the OPLS3e force field, generating about 32 stereoisomers per molecule, totaling 7369 ligands.

4.3. Docking Studies.
The pool of 7369 molecules was docked into the TRPV1 channel using the most exhaustive mode of the glide program: XP (i.e., extra precision).[38] The conformational search of the docking experiment was developed in a grid covering the vanilloid-binding site previously studied (regions I and II), with an inner box of 30 Å × 30 Å × 30 Å and an outer box of 52 Å × 52 Å × 52 Å. On average, 10 poses per ligand were reported by glide docking. All the docking poses generated were sorted by the docking energy term (DG-ligand), selecting the 70 most favorable poses that belong to different chemical modifications. These 70 CAP analogues were subjected to energy rescore by calculating the binding free energy through the molecular mechanics–generalized Born surface area (MM-GBSA) method using the prime module[39] of the Maestro/Schrödinger suite. The MM-GBSA method is an end-point method [38] to calculate the protein–ligand binding energy with a good equilibrium between accuracy in the prediction and computational cost, which consists of the sum of well-defined energy terms as follows: the MM part comprises the bonded (bond, angle, and dihedral) and nonbonded (electrostatic and van der Waals) terms. The GB and SA correspond to the polar and nonpolar contributions to the solvation-free energies, calculated from the generalized Born model and the linear relation

with the solvent-accessible solvent area (SASA), respectively. The MM-GBSA calculation comprises the prediction of the binding energy of each protein−ligand complex using an implicit solvent model (VSGB) and a minimization of all side chains of the protein in a sphere of 8 Å from the ligand.

4.4. Calculation of Pharmacokinetic Properties. Pharmacokinetic properties were calculated, including ADME. To this end, the top-ranked 24 compounds based on the calculated MM-GBSA energy were selected and analyzed using the Qikprop module of the Maestro/Schrödinger suite and pkCSM online server (http://biosig.unimelb.edu.au/pkcsm)[42] to obtain the ADME descriptors predicting their drug-like properties.[43] We evaluated six physicochemical properties: MW: molecular weight, HBA: hydrogen bond acceptor, HBD: hydrogen bond donor, Log(Po/w): octanol/water partition coefficient, RotB: rotatable bonds, SASA: Total solvent-accessible surface area, PSA: polar surface area. Furthermore, aqueous solubility (LogS), percent of human oral absorption (% HOA), skin permeability (LogKp), and apparent Caco-2 cell permeability (Caco) were used for the adsorption criterion. Brain/blood partition coefficient (LogBB), apparent MDCK cell permeability (MDCK), and central nervous system (CNS) activity were used for the distribution criterion. Metabolism was addressed by the number of likely metabolic reactions (#Metab) such as aromatic OH oxidation, enol oxidation, benzylic-like H → alcohol, allylic H → alcohol, secondary alcohol → ketone, primary alcohol → acid, tertiary alcohol E1 or SN1, amine dealkylation, ether dealkylation, pyridine C2 hydroxylation, aniline NH → NOH or NCOR, low IP—easily oxidized, alpha hydroxylation of cyclic ether, sulfoxide → sulfone, alpha hydroxylation of carbonyl, alpha, beta dehydrogenation at carbonyl, thiol SH → SSR or SR, para hydroxylation of aryl, aryl sulfide → S=O, reduction of aryl nitro to amine, oxidative deamination of primary amine, and the inhibition of cytochrome P450 isoform (CYP3A4). Finally, TC and renal organic cation transporter 2 substrate (OCT2) were used for the excretion criterion. For comparative reasons, all computed descriptors were also calculated for the CAP, CZP, and RTX molecules.

4.5. Multiparameter Scoring. To rank the best 24 CAP analogues according to their drug-like properties, we devised a MSM considering six categories: (I) Energetic (MM-GBSA binding energy), (II) physicochemical (MW, HBA, HBD, Log(Po/w), RotB, and PSA), (III) absorption (LogS, HOA, LogKp, and Caco-2), (IV) distribution (CNS, LogBB, and MDCK), (V) metabolism (#Metab, and CYP3A4), and (VI) excretion (TC and OCT2). Each predicted value was compared with its acceptance cutoff value or acceptance range values taken from Lipinski's ROF,[40] Jorgensen's ROT,[41] and Veber's rules.[42] To this end, MSM was built using the R software (version 4.0) to carry on an independent component analysis (ICA). This multivariate method decomposes the original parameters' measurements into new statistically independent variables whose effect can be considered additive.[43,44] The code is available on GitHub at https://github.com/brauchilab/Multiparameter-Scoring-Method/). During data preparation, the parameters of the CNS from the distribution category and OCT2 from the excretion category were excluded from the analysis since they did not present enough variability to help discriminate between components. To symmetrize the data distribution (*i.e.*, approximately normal) and improve model fitting, the remaining variables

for the study and their cutoff values were transformed using the Box−Cox transformation.[45] Finally, new auxiliary variables are created from the symmetrized variables, called left or right cutoff variables. Thus, we obtain four auxiliary variables from a variable subject to two cuts and two ones for variables with a single cut. For the ICA, we consider only the cutoff variables, the original variables being discarded to avoid collinearities. The analysis was carried out in two stages: by groups of characteristics and individual characteristics. For the second case, results were normalized to have weights in terms of correlations, thus facilitating their interpretation.

4.6. MD Simulations. To show the interatomic interactions that govern the affinity of our compounds with the TRPV1 channel, we select the best four CAP analogues ranked by the MSM. For this, we perform fully atomistic MD simulations, including the complexes with CAP and CZP. First, the TRPV1 structure previously used (PDB id: 7LR0), was employed as a starting point to perform molecular docking with glide program[46] in each monomer of the channel with the same parameters described in the docking procedures section (Section 2.3). The docking energy term independently chose the best pose for each CAP analogue in each monomer of the TRPV1 tetramer. The four TRPV1-CAP analogue complexes were prepared to run an NPT simulation of 100 ns without restraints. To compare the structural effect of the ligands on TRPV1, both the cryo-EM structures (PDB ids: 7LR0 and 5IS0) in complex with CAP and CZP, respectively, were simulated in the same conditions of the TRPV1−ligand complex. All the intermolecular protein−ligand interactions were calculated along the whole trajectory using the Maestro/Schrödinger suite using the default parameters such as hydrogen bonds: 2.5 Å between the donor (D) and acceptor (A) atoms and a D-hydrogen-A angle ≥120°. The water bridges are HB interactions mediated by a water molecule, with a D−A distance of 2.8 Å and a D-hydrogen-A angle ≥110°. The hydrophobic interactions (π-cation and π-π) had a cutoff distance of 4.5 Å. Ionic interactions were computed between two oppositely charged atoms with a cutoff distance of 3.7 Å.

4.7. Selectivity to Other TRPV Members. The best four CAP analogues ranked by the MSM (10A, 12A, 5A, and 1A) were tested in TRPV2, TRPV3, and TRPV4 channels. For this, we selected one representative structural file (and its amino acid sequence) for each channel from TRPV1 to TRPV4,[46] using as criteria (1) channels belonging to Mammalia, (2) best possible resolution, and (3) without mutations within the vanilloid-binding site. Thereby, we used TRPV1 (PDB id: 7LR0) of *Ictidomys tridecemlineatus* (squirrel),[9] TRPV2 (PDB id: 6OO7) of *Oryctolagus cuniculus* (rabbit),[46] TRPV3 (PDB id: 6UW6),[47] and TRPV4 (PDB id: 7AA5), both belonging to *Homo sapiens*.[48] First, similar to previous studies in the TRPV1 channel, we measured the dimensions of the vanilloid-binding site (region I) in TRPV2-4 channels, averaging the diameter between four monomers employing the same parameters used in TRPV1. In addition, we docked the best four compounds into the cryo-EM structures of TRPV2-4 channels with the same grid and docking parameters employed in TRPV1, and we used the classical modulators (CAP, CZP, and RTX) of the TRPV1 channel as controls. At most, 10 poses per molecule were obtained. We evaluated the propensity to acquire poses for each ligand within the vanilloid-binding site; for this, we calculated the percentage of each ligand within the vanilloid-binding site over the total of poses obtained for that ligand in

each channel (four docking experiments per channel in each monomer). Finally, we consider a ligand capable of binding to the vanilloid site if, for this ligand, we find at least 50% of the poses within the site in at least three monomers for each channel. Then, we compared TRPV1-4 members from different species at the sequence level to obtain the selectivity of key TRPV1 residues interacting with our analogues and their presence or absence in the other family members. All other sequences used in this work for comparative purposes were downloaded from Uniprot.[49] Multiple sequence alignments (MSAs) were performed in the Clustal Omega server[48] and Jalview editor v.2.11.1.7.[49] MSAs were used as input to evaluate the relative frequency of amino acids of the vanilloid-binding site with the WebLogo server.[50]

■ ASSOCIATED CONTENT

Ⓢ Supporting Information

The Supporting Information is available free of charge at https://pubs.acs.org/doi/10.1021/acsomega.2c05672.

ICA of groups of properties; ICA of each individual property; POV: (2S)-3-(hexadecanoyloxy)-2-[(9Z)-octadec-9-enoyloxy]propyl 2-(trimethylammonio)ethyl phosphate, 6OU: [(2~{R})-1-[2-azanylethoxy-(oxidanyl)phosphoryl]oxy-3-hexadecanoyloxy-propan-2-yl] octadic-9-enoate, PLC: diundecyl-phosphatidyl choline, and 2APB: 2-aminoethyl diphenylborinate; vanilloid-binding site dimensions; TRPV1 (PDB id: 7LR0), TRPV2 (PDB id: 6OO7), TRPV3 (PDB id: 6UW6), and TRPV4 (PDB id: 7AA5); and clustering of all docking poses: CAP (faded red−orange color), CZP (blue color), RTX (gray color), and the best four CAP analogues ranked by the MSM: 10A (magenta color), 12A (faded salmon color), 5A (red color), and 1A (yellow color) docked into the monomers B, C, and D of TRPV1 (PDB id: 7LR0), TRPV2 (PDB id: 6OO7), TRPV3 (PDB id: 6UW6), and TRPV4 (PDB id: 7AA5) channels (PDF)

■ AUTHOR INFORMATION

Corresponding Author

Bruna Benso − *Millennium Nucleus of Ion Channels Associated Diseases (MiNICAD), 8330024, Chile; School of Dentistry, Faculty of Medicine, Pontificia Universidad Católica de Chile, Santiago 8330024, Chile;* ⊙ orcid.org/ 0000-0002-4425-5174; Email: bruna.benso@uc.cl

Authors

Daniel Bustos − *Centro de Investigación de Estudios Avanzados del Maule (CIEAM), Vicerrectoría de Investigación y Postgrado, Universidad Católica del Maule, Talca 3460000, Chile; Laboratorio de Bioinformática y Química Computacional, Departamento de Medicina Traslacional, Facultad de Medicina, Universidad Católica del Maule, Talca 3480094, Chile;* ⊙ orcid.org/0000-0002-2136-2305

Christian Galarza − *Facultad de Ciencias Naturales y Matemáticas, Escuela Superior Politécnica del Litoral, ESPOL, Guayaquil 090703, Ecuador*

Wilson Ordoñez − *Facultad de Ciencias Naturales y Matemáticas, Escuela Superior Politécnica del Litoral, ESPOL, Guayaquil 090703, Ecuador*

Sebastian Brauchi − *Department of Physiology, Faculty of Medicine, Universidad Austral de Chile, Valdivia 5090000, Chile; Millennium Nucleus of Ion Channels Associated Diseases (MiNICAD), 8330024, Chile;* ⊙ orcid.org/0000-0002-8494-9912

Complete contact information is available at:
https://pubs.acs.org/10.1021/acsomega.2c05672

■ REFERENCES

(1) Damann, N.; Voets, T.; Nilius, B. TRPs in Our Senses. *Curr. Biol.* **2008**, *18*, R880−R889.
(2) Rosenbaum, T.; Simon, S. A. *TRPV1 Receptors and Signal Transduction*; CRC Press/Taylor & Francis, 2007; ISBN 0849340489.
(3) Nishida, M.; Hara, Y.; Yoshida, T.; Inoue, R.; Mori, Y. TRP Channels: Molecular Diversity and Physiological Function. *Microcirculation* **2006**, *13*, 535−550.
(4) Montell, C.; Rubin, G. M. Molecular Characterization of the Drosophila Trp Locus: A Putative Integral Membrane Protein Required for Phototransduction. *Neuron* **1989**, *2*, 1313−1323.
(5) Ribelayga, C. Vertebrate Vision: TRP Channels in the Spotlight. *Curr. Biogr.* **2010**, *20*, R278.
(6) Clapham, D. E.; Runnels, L. W.; Strübing, C. The Trp Ion Channel Family. *Nat. Rev. Neurosci.* **2001**, *2*, 387−396.
(7) Zubcevic, L. TRP Channels, Conformational Flexibility, and the Lipid Membrane. *J. Membr. Biol.* **2020**, *253*, 299−308.
(8) Clapham, D. E.; Miller, C. A Thermodynamic Framework for Understanding Temperature Sensing by Transient Receptor Potential (TRP) Channels. *Proc. Natl. Acad. Sci. U.S.A.* **2011**, *108*, 19492−19497.
(9) Nadezhdin, K. D.; Neuberger, A.; Nikolaev, Y. A.; Murphy, L. A.; Gracheva, E. O.; Bagriantsev, S. N.; Sobolevsky, A. I. Extracellular Cap Domain Is an Essential Component of the TRPV1 Gating Mechanism. *Nat. Commun.* **2021**, *12*, 1121−1128.
(10) Singh, I. P.; Bodiwala, H. S. Recent Advances in Anti-HIV Natural Products. *Nat. Prod. Rep.* **2010**, *27*, 1781−1800.

(11) Caterina, M. J. Transient Receptor Potential Ion Channels as Participants in Thermosensation and Thermoregulation. *Am. J. Physiol.* **2007**, *292*, R64−R76.

(12) Latorre, R.; Zaelzer, C.; Brauchi, S. Structure-Functional Intimacies of Transient Receptor Potential Channels. *Q. Rev. Biophys.* **2009**, *42*, 201−246.

(13) Liao, M.; Cao, E.; Julius, D.; Cheng, Y. Structure of the TRPV1 Ion Channel Determined by Electron Cryo-Microscopy. *Nature* **2013**, *504*, 107−112.

(14) Bamps, D.; Vriens, J.; de Hoon, J.; Voets, T. TRP Channel Cooperation for Nociception: Therapeutic Opportunities. *Annu. Rev. Pharmacol. Toxicol.* **2021**, *61*, 655−677.

(15) Julius, D.; Nathans, J. Signaling by Sensory Receptors. *Cold Spring Harb. Perspect. Biol* **2012**, *4*, a005991.

(16) Chu, Y.; Cohen, B. E.; Chuang, H. A Single TRPV1 Amino Acid Controls Species Sensitivity to Capsaicin. *Sci. Rep.* **2020**, *10*, 11−12.

(17) Jordt, S. E.; Julius, D. Molecular Basis for Species-Specific Sensitivity to "Hot" Chili Peppers. *Cell* **2002**, *108*, 421−430.

(18) Nilius, B.; Owsianik, G. Transient Receptor Potential Channelopathies. *Eur. J. Appl. Physiol.* **2010**, *460*, 437−450.

(19) Premkumar, L. S.; Sikand, P. TRPV1 A Target for Next Generation Analgesics. *Curr. Neuropharmacol.* **2008**, *6*, 151.

(20) Jara-Oseguera, A.; Islas, L. D. The Role of Allosteric Coupling on Thermal Activation of Thermo-TRP Channels. *Biophys. J.* **2013**, *104*, 2160−2169.

(21) Gao, Y.; Cao, E.; Julius, D.; Cheng, Y. TRPV1 Structures in Nanodiscs Reveal Mechanisms of Ligand and Lipid Action. *Nature* **2016**, *534*, 347−351.

(22) Yang, F.; Zheng, J. Understand Spiciness: Mechanism of TRPV1 Channel Activation by Capsaicin. *Protein Cell* **2017**, *8*, 169−177.

(23) Vu, S.; Singh, V.; Wulff, H.; Yarov-Yarovoy, V.; Zheng, J. New Capsaicin Analogs as Molecular Rulers to Define the Permissive Conformation of the Mouse Trpv1 Ligand-Binding Pocket. *eLife* **2020**, *9*, 1−17.

(24) Walpole, C. S. J.; Wrigglesworth, R.; Bevan, S.; Campbell, E. A.; Dray, A.; James, I. F.; Perkins, M. N.; Reid, D. J.; Winter, J. Analogs of Capsaicin with Agonist Activity as Novel Analgesic Agents; Structure-Activity Studies. 1. The Aromatic "A-Region". *J. Med. Chem.* **1993**, *36*, 2362−2372.

(25) Walpole, C. S. J.; Bevan, S.; Bovermann, G.; Boelsterli, J. J.; Breckenridge, R.; Davies, J. W.; Hughes, G. A.; James, I.; Oberer, L.; Winter, J.; et al. The Discovery of Capsazepine, the First Competitive Antagonist of the Sensory Neuron Excitants Capsaicin and Resiniferatoxin. *J. Med. Chem.* **2002**, *37*, 1942−1954.

(26) Pérez-González, A.; Prejanò, M.; Russo, N.; Marino, T.; Galano, A. Capsaicin, a Powerful ●OH-Inactivating Ligand. *Antioxidants* **2020**, *9*, 1247.

(27) Gavva, N. R.; Klionsky, L.; Qu, Y.; Shi, L.; Tamir, R.; Edenson, S.; Zhang, T. J.; Viswanadhan, V. N.; Toth, A.; Pearce, L. v.; et al. Molecular Determinants of Vanilloid Sensitivity in TRPV1. *J. Biol. Chem.* **2004**, *279*, 20283−20295.

(28) Benso, B.; Bustos, D.; Zarraga, M. O.; Gonzalez, W.; Caballero, J.; Brauchi, S. Chalcone Derivatives as Non-Canonical Ligands of TRPV1. *Int. J. Biochem. Cell Biol.* **2019**, *112*, 18−23.

(29) Nadezhdin, K. D.; Neuberger, A.; Nikolaev, Y. A.; Murphy, L. A.; Gracheva, E. O.; Bagriantsev, S. N.; Sobolevsky, A. I. Extracellular Cap Domain Is an Essential Component of the TRPV1 Gating Mechanism. *Nat. Commun.* **2021**, *12*, 1121−1128.

(30) Wong, G. Y.; Gavva, N. R. Therapeutic Potential of Vanilloid Receptor TRPV1 Agonists and Antagonists as Analgesics: Recent Advances and Setbacks. *Brain Res.* **2009**, *60*, 267−277.

(31) Fattori, V.; Hohmann, M. S. N.; Rossaneis, A. C.; Pinho-Ribeiro, F. A.; Verri, W. A. Capsaicin: Current Understanding of Its Mechanisms and Therapy of Pain and Other Pre-Clinical and Clinical Uses. *Molecules* **2016**, *21*, 844.

(32) Berman, H. M.; Westbrook, J.; Feng, Z.; Gilliland, G.; Bhat, T. N.; Weissig, H.; Shindyalov, I. N.; Bourne, P. E. The Protein Data Bank. *Nucleic Acids Res.* **2000**, *28*, 235−242.

(33) QikProp Schrödinger Available online. https://www.schrodinger.com/products/qikprop (accessed on October 9, 2021).

(34) Søndergaard, C. R.; Olsson, M. H. M.; Rostkowski, M.; Jensen, J. H. Improved Treatment of Ligands and Coupling Effects in Empirical Calculation and Rationalization of PKa Values. *J. Chem. Theory Comput.* **2011**, *7*, 2284−2295.

(35) Berendsen, H. J. C.; Postma, J. P. M.; van Gunsteren, W. F.; Hermans, J. *Interaction Models for Water in Relation to Protein Hydration*, 1981; pp 331−342.

(36) Roos, K.; Wu, C.; Damm, W.; Reboul, M.; Stevenson, J. M.; Lu, C.; Dahlgren, M. K.; Mondal, S.; Chen, W.; Wang, L.; et al. OPLS3e: Extending Force Field Coverage for Drug-Like Small Molecules. *J. Chem. Theory Comput.* **2019**, *15*, 1863−1874.

(37) Smart, O. S.; Goodfellow, J. M.; Wallace, B. A. The Pore Dimensions of Gramicidin A. *Biophys. J.* **1993**, *65*, 2455.

(38) Friesner, R. A.; Murphy, R. B.; Repasky, M. P.; Frye, L. L.; Greenwood, J. R.; Halgren, T. A.; Sanschagrin, P. C.; Mainz, D. T. Extra precision glide: docking and scoring incorporating a model of hydrophobic enclosure for protein-ligand complexes. *J. Med. Chem.* **2006**, *49*, 6177−6196.

(39) Jacobson, M. P.; Pincus, D. L.; Rapp, C. S.; Day, T. J. F.; Honig, B.; Shaw, D. E.; Friesner, R. A. A Hierarchical Approach to All-Atom Protein Loop Prediction. *Proteins* **2004**, *55*, 351−367.

(40) Lipinski, C. A.; Lombardo, F.; Dominy, B. W.; Feeney, P. J. Experimental and Computational Approaches to Estimate Solubility and Permeability in Drug Discovery and Development Settings. *Adv. Drug Deliv. Rev.* **2001**, *46*, 3−26.

(41) Jorgensen, W. L. The Many Roles of Computation in Drug Discovery. *Science* **2004**, *303*, 1813−1818.

(42) Veber, D. F.; Johnson, S. R.; Cheng, H. Y.; Smith, B. R.; Ward, K. W.; Kopple, K. D. Molecular Properties That Influence the Oral Bioavailability of Drug Candidates. *J. Med. Chem.* **2002**, *45*, 2615−2623.

(43) Hyvärinen, A. Independent Component Analysis: Recent Advances. *Philos. Trans. R. Soc., A* **2013**, *371*, 20110534.

(44) Box, G. E. P.; Cox, D. R. An Analysis of Transformations. *J. Roy. Stat. Soc. B* **1964**, *26*, 211−243.

(45) Pumroy, R. A.; Samanta, A.; Liu, Y.; Hughes, T. E. T.; Zhao, S.; Yudin, Y.; Rohacs, T.; Han, S.; Moiseenkova-Bell, V. Y. Molecular Mechanism of TRPV2 Channel Modulation by Cannabidiol. *eLife* **2019**, *8*, No. e48792.

(46) Deng, Z.; Maksaev, G.; Rau, M.; Xie, Z.; Hu, H.; Fitzpatrick, J. A. J.; Yuan, P. Gating of Human TRPV3 in a Lipid Bilayer. *Nat. Struct. Biol.* **2020**, *27*, 635−644.

(47) Deng, Z.; Paknejad, N.; Maksaev, G.; Sala-Rabanal, M.; Nichols, C. G.; Hite, R. K.; Yuan, P. Cryo-EM and X-Ray Structures of TRPV4 Reveal Insight into Ion Permeation and Gating Mechanisms. *Nat. Struct. Biol* **2018**, *25*, 252−260.

(48) Waterhouse, A. M.; Procter, J. B.; Martin, D. M. A.; Clamp, M.; Barton, G. J. Jalview Version 2—a Multiple Sequence Alignment Editor and Analysis Workbench. *Bioinformatics* **2009**, *25*, 1189−1191.

(49) Crooks, G. E.; Hon, G.; Chandonia, J.-M.; Brenner, S. E. WebLogo: A Sequence Logo Generator. *Genome Res.* **2004**, *14*, 1188−1190.

(50) Nadezhdin, K. D.; Neuberger, A.; Trofimov, Y. A.; Krylov, N. A.; Sinica, V.; Kupko, N.; Vlachova, V.; Zakharian, E.; Efremov, R. G.; Sobolevsky, A. I. Structural Mechanism of Heat-Induced Opening of a Temperature-Sensitive TRP Channel. *Nat. Struct. Biol.* **2021**, *28*, 564−572.

(51) Kwon, D. H.; Zhang, F.; Suo, Y.; Bouvette, J.; Borgnia, M. J.; Lee, S.-Y. Heat-Dependent Opening of TRPV1 in the Presence of Capsaicin. *Nat. Struct. Biol.* **2021**, *28*, 554.

(52) Gianti, E.; Klein, M. L.; Rohacs, T.; Carnevale, V. Activation of TRPV1 by Lipids: Can Lipid Tails Bridge the Gap between the Vanilloid Binding Site and the Peripheral Cavities? *Biophys. J.* **2019**, *116*, 536a.

(53) Yazici, A. T.; Gianti, E.; Kasimova, M. A.; Lee, B.-H.; Carnevale, V.; Rohacs, T. Dual Regulation of TRPV1 Channels by Phosphatidylinositol via Functionally Distinct Binding Sites. *J. Biol. Chem.* **2021**, *296*, 100573−100574.

(54) Yang, F.; Xiao, X.; Cheng, W.; Yang, W.; Yu, P.; Song, Z.; Yarov-Yarovoy, V.; Zheng, J. Structural Mechanism Underlying Capsaicin Binding and Activation of the TRPV1 Ion Channel. *Nat. Chem. Biol.* **2015**, *11*, 518−524.

(55) Elokely, K.; Velisetty, P.; Delemotte, L.; Palovcak, E.; Klein, M. L.; Rohacs, T.; Carnevale, V. Understanding TRPV1 Activation by Ligands: Insights from the Binding Modes of Capsaicin and Resiniferatoxin. *Proc. Natl. Acad. Sci. U.S.A.* **2016**, *113*, E137−E145.

(56) Veber, D. F.; Johnson, S. R.; Cheng, H. Y.; Smith, B. R.; Ward, K. W.; Kopple, K. D. Molecular Properties That Influence the Oral Bioavailability of Drug Candidates. *J. Med. Chem.* **2002**, *45*, 2615−2623.

(57) Lionta, E.; Spyrou, G.; Vassilatis, D. K.; Cournia, Z. Structure-Based Virtual Screening for Drug Discovery: Principles, Applications and Recent Advances. *Curr. Top. Med. Chem.* **2014**, *14*, 1923.

(58) Zhivkova, Z.; Doytchinova, I. Quantitative Structure-Clearance Relationships of Acidic Drugs. *Mol. Pharm.* **2013**, *10*, 3758−3768.

(59) Singh, A. K.; McGoldrick, L. L.; Sobolevsky, A. I. Structure and Gating Mechanism of the Transient Receptor Potential Channel TRPV3. *Nat. Struct. Biol.* **2018**, *25*, 805−813.

(60) Neuberger, A.; Nadezhdin, K. D.; Zakharian, E.; Sobolevsky, A. I. Structural Mechanism of TRPV3 Channel Inhibition by the Plant-Derived Coumarin Osthole. *EMBO Rep.* **2021**, *22*, No. e53233.

(61) Gees, M.; Colsoul, B.; Nilius, B. The Role of Transient Receptor Potential Cation Channels in Ca2+ Signaling. *Cold Spring Harbor Perspect. Biol.* **2010**, *2*, a003962.

(62) Nelson, E. K.; Dawson, D. E. The constitution of capsaicin, the pungent principle of capsicum III. *J. Am. Chem. Soc.* **2002**, *45*, 2179−2181.

(63) Reyes-Escogido, M.; Gonzalez-Mondragon, E. G.; Vazquez-Tzompantzi, E. Chemical and Pharmacological Aspects of Capsaicin. *Molecules* **2011**, *16*, 1253−1270.

(64) Chou, M. Z.; Mtui, T.; Gao, Y. D.; Kohler, M.; Middleton, R. E. Resiniferatoxin Binds to the Capsaicin Receptor (TRPV1) near the Extracellular Side of the S4 Transmembrane Domain. *Biochemistry* **2004**, *43*, 2501−2511.

(65) Backes, W. L. Pharmacokinetics. *xPharm: The Comprehensive Pharmacology Reference*; Elsevier, 2007; Vol. 1.

(66) Li, Y.; Meng, Q.; Yang, M.; Liu, D.; Hou, X.; Tang, L.; Wang, X.; Lyu, Y.; Chen, X.; Liu, K.; et al. Current Trends in Drug Metabolism and Pharmacokinetics. *Acta Pharm. Sin. B.* **2019**, *9*, 1113−1144.

(67) Lin, J.; Sahakian, D.; de Morais, S.; Xu, J.; Polzer, R.; Winter, S. The Role of Absorption, Distribution, Metabolism, Excretion and Toxicity in Drug Discovery. *Curr. Top. Med. Chem.* **2003**, *3*, 1125−1154.

(68) Daina, A.; Michielin, O.; Zoete, V. SwissADME: A Free Web Tool to Evaluate Pharmacokinetics, Drug-Likeness and Medicinal Chemistry Friendliness of Small Molecules. *Sci. Rep.* **2017**, *7*, 42717.

(69) Guan, L.; Yang, H.; Cai, Y.; Sun, L.; Di, P.; Li, W.; Liu, G.; Tang, Y. ADMET-Score—a Comprehensive Scoring Function for Evaluation of Chemical Drug-Likeness. *MedChemComm* **2019**, *10*, 148−157.